HER storage ring transformations to obtain longitudinal polarization of electrons at the SuperKEKB interaction point

I.A.Koop, A.V. Otboev, Yu.M. Shatunov, BINP SB RAS, 630090 Novosibirsk

Introduction

This paper discusses the problems of obtaining longitudinal polarization in future experiments of the BELLE-2 collaboration at the SuperKEKB electron-positron collider [1].

Due to the extremely small coupling coefficient of transverse oscillations in SuperKEKB [2, 3]: $\varepsilon_y/\varepsilon_x \approx 0.002$, it seems absolutely impossible to use any spin rotator schemes using transverse dipole fields. Only the scheme with the use of a longitudinal magnetic field has no effect on the value of the vertical emittance, which is formed by quantum fluctuations of synchrotron radiation in the main dipole magnets of the ring and by parasitic coupling of transverse oscillations.

The concept of a scheme for obtaining longitudinal polarization

Below, we discuss the simplest version of such a scheme of rotations of the direction of the electron spin vector, when the vertical direction of the spin in the main arcs is completely restored when the beam passes through a long experimental straight section of the HER ring [4, 5], see Fig. 1.

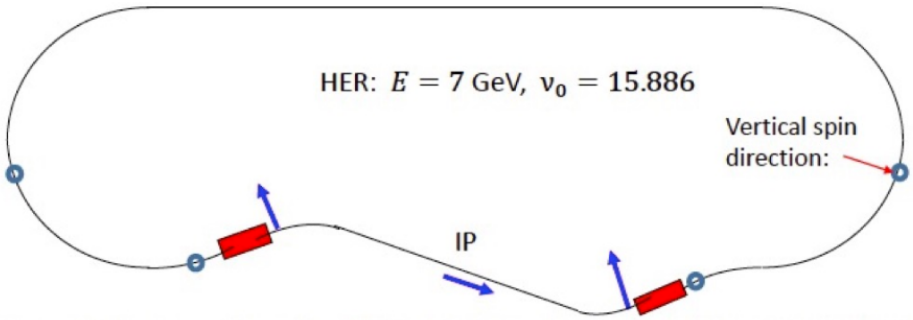

Spin direction is vertical in the main part of HER. Then it is rotated to the horizontal plane by the set of two solenoids, which are comprising the 90^0 spin rotator.

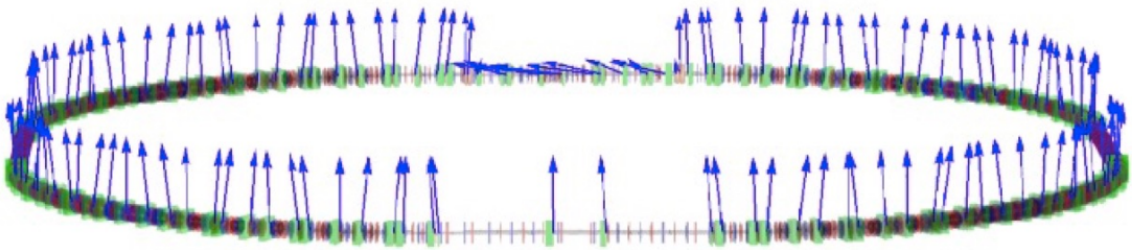

Fig. 1 Scheme of spin rotations with restoration of their vertical direction in the main arcs of the ring. Each spin rotator consists of two solenoids and several skew-quadrupole lenses that compensate for the coupling of betatron oscillations introduced by these solenoids.

The left and right spin rotators have the opposite sign of the longitudinal magnetic field, and the whole rotation scheme is generally antisymmetric in the signs of magnetic fields at an equilibrium orbit. This antisymmetry ensures almost complete absence of the dependence of the spin orientation in the loops on the particle energy, which is very important for obtaining a long beam depolarization time. The presence of a nonzero dispersion function in spin rotators and magnets between them does not allow to completely suppress the chromatic energy dependence of the spin orbit in the loops. We will discuss this issue in greater details later.

To rotate the electron spin by 90 degrees, the field integral in the solenoids is proportional to the particle momentum:

$$Bl = \frac{\pi}{2(1+a_e)}BR$$

Here $BR = pc/e$ - magnetic rigidity, $a_e \approx 1.16 \cdot 10^{-3}$ – anomalous magnetic moment of an electron.

The subsequent rotation of the spin by 90^0 in the horizontal plane occurs in the section from the rotator to the point of intersection of the beams with the total angle of rotation of the velocity vector equal to:

$$\theta = \frac{\pi}{2\nu_0}$$

where $\nu_0 = \gamma a_e$ is the dimensionless spin frequency (or tune) proportional to the gamma factor of the particle.

To detune from resonances with betatron oscillation frequencies, which can quickly depolarize the beam due to beam-beam collision effects, we chose the optimal value of the electron energy equal to $E = 7.15$ GeV, which corresponds to the spin tune $\nu_0 = 16.226$ – sufficiently distant both from close to half-integer values of transverse oscillation frequencies, and from integer resonances with their synchrotron satellites. This value of the spin tune dictates to us the required total angle of all turns in the horizontal plane from the rotator to the interaction point equal to $\theta = 0.0968$.

In the current geometry of the complicated wavy HER orbit, there is no suitable place for a spin rotator. Moreover, given that the length of the rotator is about 10 meters, several dipoles had to be moved from their places, simultaneously changing their angles of rotation. Such transformations of the long insertion connecting the left and right arches were calculated and optimized taking into account the preservation of the storage ring perimeter. The geometries of the separation of the trajectories of the LER and HER rings are slightly different on the left and right sides from the interaction point, see respectively Fig. 2 and Fig. 3.

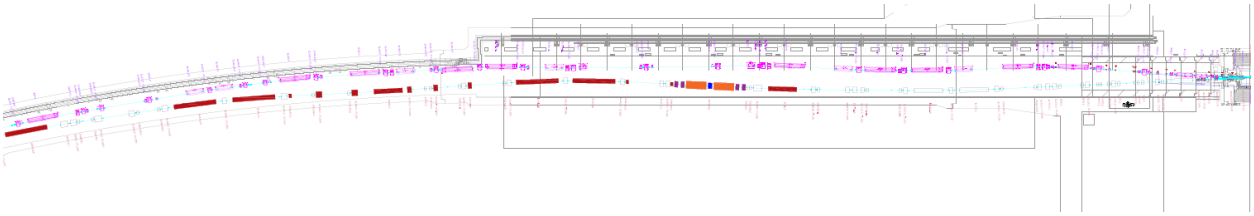

Fig. 2 To the left from the IP half of experimental straight section. The modified magnetic elements of the HER ring are painted in dark brown, and the solenoids of the spin rotator are painted in dark yellow. The distance between the rings is great enough everywhere.

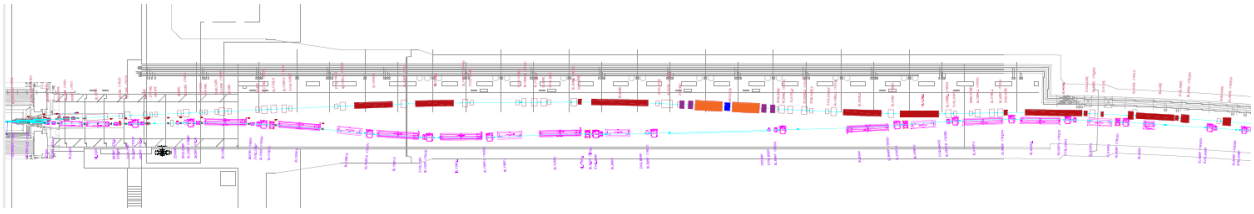

Fig. 3 To the right from the IP half of straight section. At the entrance to the tunnel, the magnets of the rings are very close, but all technical problems can obviously be solved.

In a condensed form, the scheme of intersection of the collider rings is shown in Fig. 4.

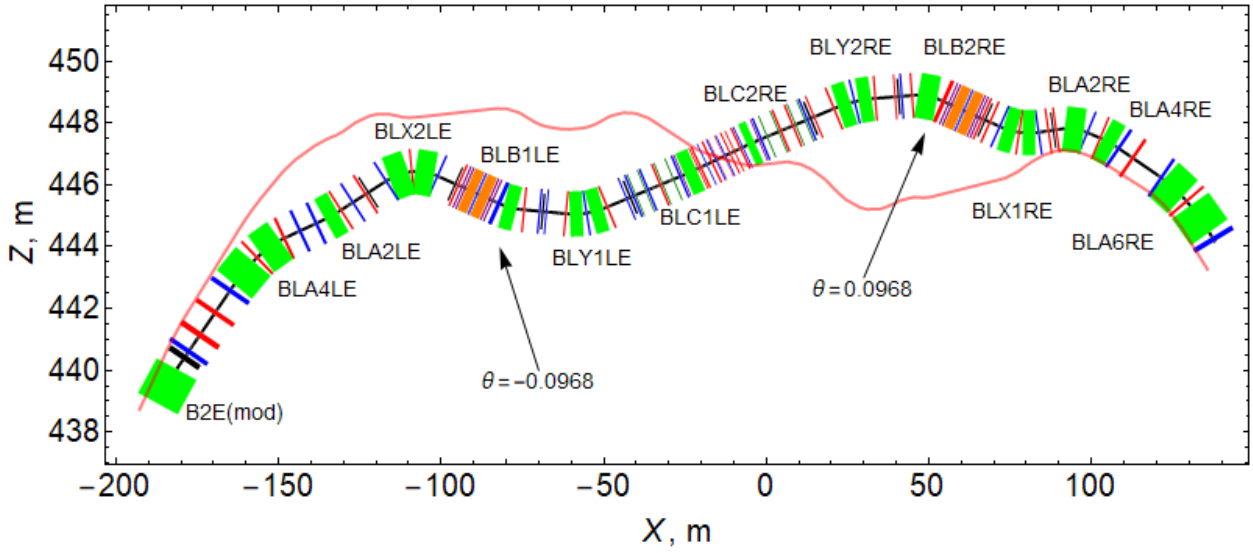

"B2E(mod)"	"BLA2LE"	"BLA2RE"	"BLA4LE"	"BLA4RE"	"BLA6RE"	"BLB1LE"
0.0745895	−0.0181419	0.0591537	0.0520765	0.0280687	0.0501498	−0.0368136
"BLB2RE"	"BLC1LE"	"BLC2RE"	"BLX1RE"	"BLX2LE"	"BLY1LE"	"BLY2RE"
0.0548871	−0.00591049	0.0059199	−0.0310501	0.0570931	−0.0270415	0.018

Fig.4 Optimized SuperKEKB ring intersection scheme for longitudinal polarization. Spin rotators are located in convenient places, away from the tunnel walls and the magnetic elements of the positron ring. The angles of rotation of all dipole magnets are given at the bottom of the diagram, and in Tables 1 and 2. The lengths and angles of only modified dipoles are given.

Table 1. Lengths and rotation angles of the dipoles to the left of the intersection of the beams.

		Original parameters of dipoles		New parameters	
Name	Quantity	Length, m	Angle, rad	Length, m	Angle, rad
B2E.4	1	5.90220	0.0557427	5.90220	0.0745895
BLA4LE	2	5.90220	0.0663658	5.90220	0.0520765
BLA2LE	1	5.90220	0.0206421	3.96143	- 0.0181419
BLX2LE	2	3.96143	0.0259281	5.90220	0.0570931
BLB1LE	1	3.96143	-0.0229996	3.96143	-0.0368136

Table 2. Lengths and rotation angles of the dipoles to the right of the intersection of the beams.

		Original parameters of dipoles		New parameters	
Name	Quantity	Length, m	Angle, rad	Length, m	Angle, rad
BLA6RE	2	5.90220	0.0501497	5.90220	0.0501498
BLA4RE	1	5.90220	0.0480687	3.96143	0.0280687
BLA2RE	1	3.96143	0.0348280	5.90220	0.0591537
BLX1RE	2	3.96143	-0.0221788	3.96143	-0.0310501
BLB2RE	1	3.96143	0.0234696	5.90220	0.0548871
BLY2RE	2	3.96143	0.0270000	3.96143	0.0180000

Note that due to a significant change in some of the rotation angles, the lengths of the corresponding dipoles also changed. In the new scheme, the number of long dipoles is increased by two units, while the number of short dipoles is decreased also by two units. We note that the right half of the long experimental region in the new geometry is lengthened by 14 mm, which is fully compensated by the corresponding shortening of its left half. Spin rotators are inserted into specially widened gaps about 10 m long, between the structural blocks of compensation for the local chromaticity of the triplets of the strong final quadrupole lenses. Each such SX or SY-block [2] consists of a pair of identical dipole magnets and symmetrically spaced quadrupole lenses, which provide minus-unity of the diagonal elements of the transport matrix of the section between the centers of the same sextupole lenses $T_{11} = T_{22} = T_{33} = T_{44} = -1$. Also in this matrix the elements $T_{12} = T_{34} = 0$ equal to zero. Such optics ideally provide complete suppression of geometric aberrations for particles with equilibrium energy. This scheme of compensation for the local chromaticity of strong lenses of the final focus by pairs of non-interleaved sextupoles is currently generally accepted and we have kept this approach intact, changing only the dipole angles in both chromatic blocks.

Spin rotators.

There are several options for compensating for the coupling of betatron oscillations introduced by the longitudinal magnetic field of the solenoids. The general idea is that in a system of reference, which rotates with a half Larmor frequency $\kappa(s) = B_s/2BR$ around the longitudinal axis, motion in two transverse degrees of freedom become uncoupled if the angles of rotation of all skew-quadrupole lenses around their axis are chosen equal to the integral of such twist [6]:

$$\varphi(s) = \int_{s0}^{s} \kappa(s) ds$$

Here, the reference longitudinal coordinate $s0$ is chosen in such a way that exactly half of the integral of the longitudinal field over the entire rotator is accumulated from the beginning of the rotator to this point. As a result, the angles of rotation of lenses at azimuths $s > s0$ have a sign determined by the sign of the torsion $\kappa(s)$, while lenses at azimuths $s < s0$ are rotated around their axis in the opposite direction.

In the thus introduced rotating Cartesian coordinate system (x, y, s), the equations of motion for transverse deflections x, y take on an extremely simple form:

$$x'' + (\kappa(s)^2 + g(s))x = 0$$
$$y'' + (\kappa(s)^2 - g(s))y = 0$$

where $g(s) = G(s)/BR$ is the transverse field gradient normalized to the magnetic rigidity. It is shown in [6] that the full 4x4 transport matrix of a spin rotator has zero anti-diagonal 2x2 blocks if the matrices for x, y oscillations counted in the rotating coordinate system are equal to each other with the opposite sign: $T_x = -T_y = T$. Under this condition, the full matrix *M* of the rotator has the same form both in the rotating basis and in the fixed one:

$$M = \begin{pmatrix} T & 0 \\ 0 & -T \end{pmatrix}$$

Note that there is great freedom in choosing the form of 2x2 matrices$T_x = -T_y = T$. In our choice, we settled on a mirror-symmetric arrangement of lenses and two sections of solenoids, shown in Fig. 5. Rotator optics based on such a scheme was successfully implemented in the 90-

s on the AmPS storage ring at NIKHEF, Amsterdam [7].

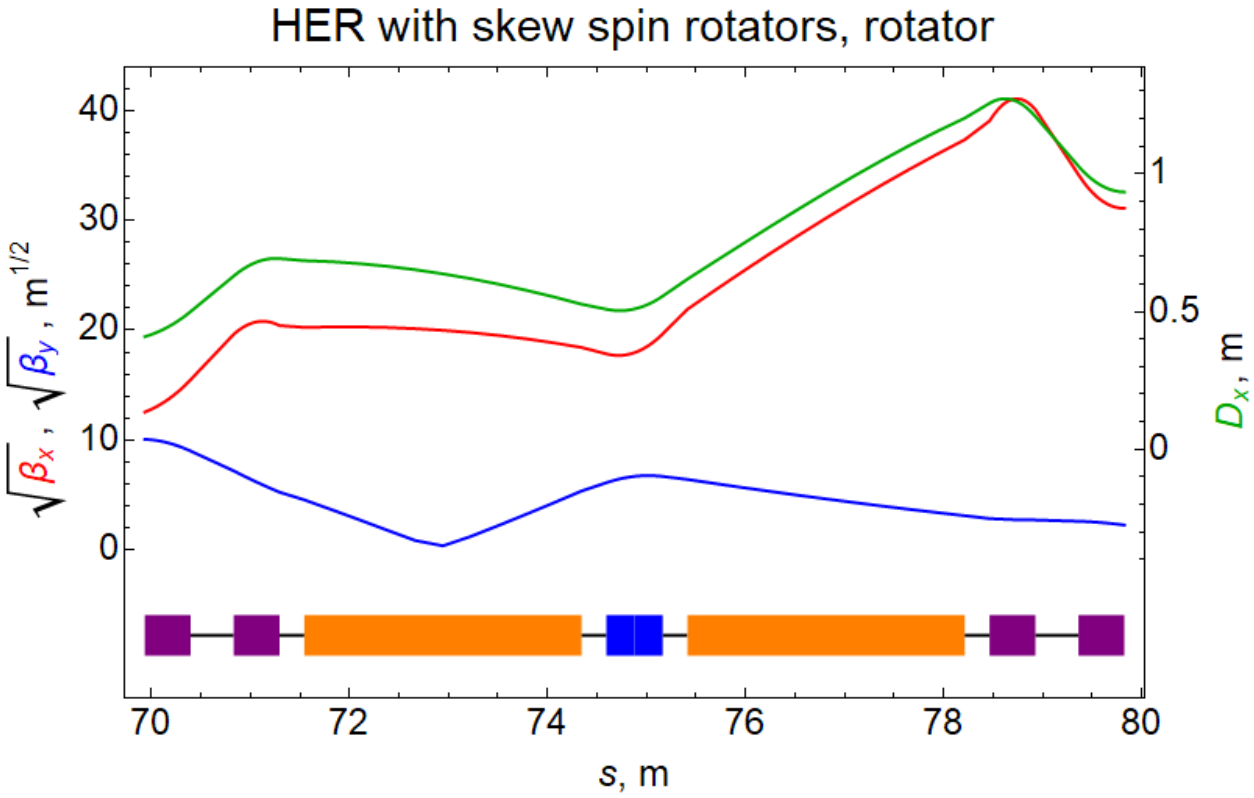

Fig. 5 Optical functions of the spin rotator for the left half of the long interaction region.

The middle lens is not rotated around its axis, while the lenses of the two outermost doublets are rotated at an angle $\varphi = \pm\pi/8(1 + a_e) = \pm\, 22.474^0$.

The *X*-box 2x2 matrix is:

$$T = \begin{pmatrix} 0.4134 & 7.13 \\ -0.14025 & 0.4134 \end{pmatrix}$$

The total length of the rotator is 9.89112 meters. Table 3 shows the main parameters of the solenoids and lenses of this spin rotator.

Table 3. Basic parameters of lenses and solenoids for *BR* = 23.3495 T·m (*E* = 7.15 GeV).

Element	Length, m	Field or Gradient: T, T/m
Quadrupole #1, #5	0.46227	-29.4792 ($\varphi 1 = -\varphi 5 = -22.474^0$)
Drift 1	0.436	
Quadrupole #2, #4	0.46227	28.5569 ($\varphi 2 = -\varphi 4 = -22.474^0$)
Drift 2	0.25	
Solenoid	2.8	6.54197
Drift 3	0.25	
Quadrupole #3	0.57004	-25.3736 ($\varphi 3 = 0$)

Alternatively, we consider the option of combining the solenoidal and quadrupole fields. This approach has already been discussed in [5], but with a more radical proposal - to combine three types of fields: solenoidal, quadrupole, and dipole. But, as we have already said, the presence

of a dipole field leads to the excitation of too large vertical emittance. Table 4 shows the parameters of quadrupole lenses of such a combined version, in which the solenoidal field is continuous and occupies the entire length of the rotator of 9.2 m.

The windings of the quadrupole lenses are superimposed on a cylindrical mandrel over the solenoid winding. Moreover, there are two sets of windings: straight-oriented windings and weaker second windings rotated at an angle of 45^0 to them, creating a skew-quadrupole field. The total number of lenses in the rotator is increased to 7 in order to have the freedom to reproduce the same optics in the versions with the longitudinal field on and off.

Table 4. Basic parameters of lenses and solenoids of a spin rotator with a superposition of solenoidal and quadrupole fields for *BR* = 23.3495 T·m (*E* = 7.15 GeV). The sequence of numbering of structure elements: 1, 2,…, 17.

Element	Length, m	Field or Gradient: T, T/m
Drift #1, #17	0.34556	$B_s = G = 0$
Pure Solenoid #2, #16	0.15	$B_s = 4.067373$
Quadrupole plus Solenoid: #3, #15	0.7	-20.067768 ($\varphi 3 = -\varphi 15 = -19.822^0$)
Solenoid #4, #14	0.4	$B_s = 4.067373$
Quadrupole plus Solenoid: #5, #13	0.7	23.232294 ($\varphi 5 = -\varphi 13 = -14.5297^0$)
Solenoid #6, #12	0.8	$B_s = 4.067373$
Quadrupole plus Solenoid: #7, #11	0.7	-5.385630 ($\varphi 7 = -\varphi 11 = -7.3598^0$)
Solenoid #8, 10	0.8	
Quadrupole plus Solenoid: #9	0.7	-22.806964 ($\varphi 9 = 0$)

The option with combined fields has several attractive points. Its main advantage over the variant with separated functions is the small value of the longitudinal field: $B_s = 4.067373$ T versus alternative $B_s = 6.54197$ T. Also, the use of a common cylindrical frame supporting both the solenoidal and quadrupole windings may be more technologically advanced as compared to their separate fixation in space. In addition, the need to create two types of lens windings - straight-oriented and skew-rotated - makes the cosine-theta technology the preferred choice.

When calculating the transport matrix of a section of the structure with superposition of the quadrupole and solenoidal fields constant along s, we used numerical methods for calculating the exponent of the matrix of a linear system of equations of motion:

$$\frac{dX}{ds} = A \cdot X \qquad A = \begin{pmatrix} 0 & 1 & \kappa & 0 \\ -\kappa^2 - g & 0 & 0 & \kappa \\ -\kappa & 0 & 0 & 1 \\ 0 & -\kappa & -\kappa^2 + g & 0 \end{pmatrix}$$

Transformation transport matrix of vector $X = (x, p_x, y, p_y)^T$ is equal:

$$T(s, g, \kappa) = R(-s\kappa)\exp(sA)R(s\kappa)$$

where $R(s\kappa)$ – the rotation matrix, and the arguments of the matrix A are as defined above. Note that p_x and p_y are canonical momenta, defined as:

$$p_x = x' - \kappa y$$
$$p_y = y' + \kappa x$$

Canonical momenta do not experience any jumps at the boundaries of the solenoidal field, in contrast to kinetic impulses x', y', which subjected a discontinuity at solenoid edges.

The angles of rotation of the lenses were selected in such a way as to make all elements of antidiagonal 2x2 coupling boxes of the complete transport matrix of the rotator vanish. To fulfill this condition, taking into account the mirror symmetry of the placement of all seven lenses and with the antisymmetric rotation of six of them around the axis, we used a procedure for numerical optimization of three rotation angles and gradients of four lens families (the central lens is not rotated!). The *X*-block matrix was selected the same as in the rotator version with separated longitudinal and transverse fields:

$$T = \begin{pmatrix} 0.4134 & 7.13 \\ -0.14025 & 0.4134 \end{pmatrix}$$

The matrix of the *Y*-block is equal to it with the opposite sign.

At the edges of the rotator, short drift gaps with a length of 0.34556 m are left free from fields, connecting the cold superconducting magnetic system with room temperature of the adjacent areas. The total length of the entire rotator is 9.89112 m, same as in the first version.

Beam depolarization time.

When a photon of synchrotron radiation is emitted, there is an abrupt change in the equilibrium direction of the spin and the magnitude of the projection of the spin on the new equilibrium direction. The spin relaxation time of the beam due to this process and the equilibrium degree of polarization are determined by the well-known Derbenev-Kondratenko formulas [10]:

$$\tau_{rad}^{-1} = \frac{5\sqrt{3}}{8}\lambda_e r_e c\gamma^5 \left\langle |r|^{-3}\left(1 - \frac{2}{9}(\vec{n}\vec{v})^2 + \frac{11}{18}\left(\vec{d}\right)^2\right)\right\rangle$$

$$\xi_{rad} = -\frac{8}{5\sqrt{3}}\frac{\langle |r|^{-3}\vec{b}(\vec{n} - \vec{d})\rangle}{\left\langle |r|^{-3}\left(1 - \frac{2}{9}(\vec{n}\vec{v})^2 + \frac{11}{18}\left(\vec{d}\right)^2\right)\right\rangle}$$

where $\lambda_e, r_e,\ c$ and γ – Compton wavelength of an electron, its classical radius, speed of light and gamma factor, respectively. Other parameters stands for: r – radius of curvature of the orbit at the point of emission of the photon, $\vec{b}$ – unit vector indicating the direction of the magnetic field, $\vec{n}$ - unit vector along the equilibrium spin direction at a given azimuth, $\vec{d} = \gamma(d\vec{n}/d\gamma)$ – spin-orbit coupling vector, showing the direction of the jump of vector $\vec{n}$ when a photon is emitted, and the magnitude of this jump.

Modulus distribution of vector $\vec{d}$ over the azimuth of the storage ring was calculated by the ASPIRRIN program, created in the 90s [8, 9]. Figure 6 shows the graph $\left|\vec{d}(s)\right|$ calculated for the

rotator optics option with the parameters in Table 3.

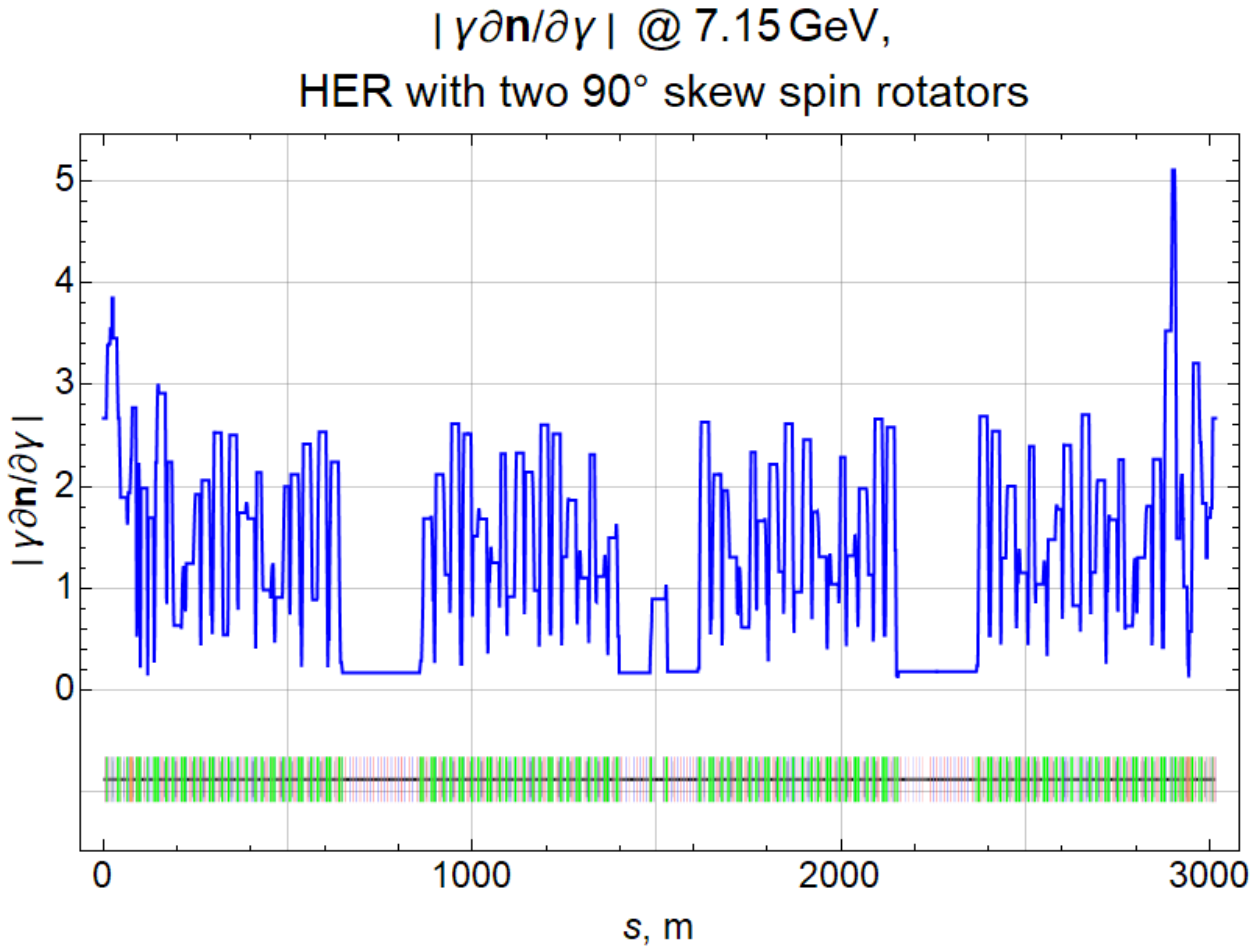

Fig.6 Graph of the modulus of the spin-orbit coupling vector in the HER ring with a modified rotation geometry in the experimental section. Rotator parameters from Table 3 and Fig. 5.

It is essential that for a given optimized value of the beam energy *E* = 7.15 GeV the modulus $|\vec{d}(s)|$ almost everywhere does not exceed the factor 2. Thereby the spin relaxation time falls from the initial values of the Sokolov-Ternov polarization time $\tau_{ST} = 32000$ s only to quite acceptable $\tau_{rad} = 10000$ s. This time remains very long in comparison with the time for refreshing the beam with new polarized electrons, which is less than $\tau_{beam} < 1000$ sec. The energy dependence of the radiation spin relaxation time is shown in Fig. 7. Resonances with integer values of the spin frequency occurred at the energy *E* = 6.61, 7.05, 7.49 GeV, and the so-called “intrinsic” spin resonances with the betatron vibration frequencies are located at the spin tunes $\{\nu_0\}$ =0.4 and 0.6. You have to choose the beam energy and operate somewhere in between these two types of resonances, for example at *E*=7.15 GeV, or in other words at spin tune $\nu_0 = 16.226$.

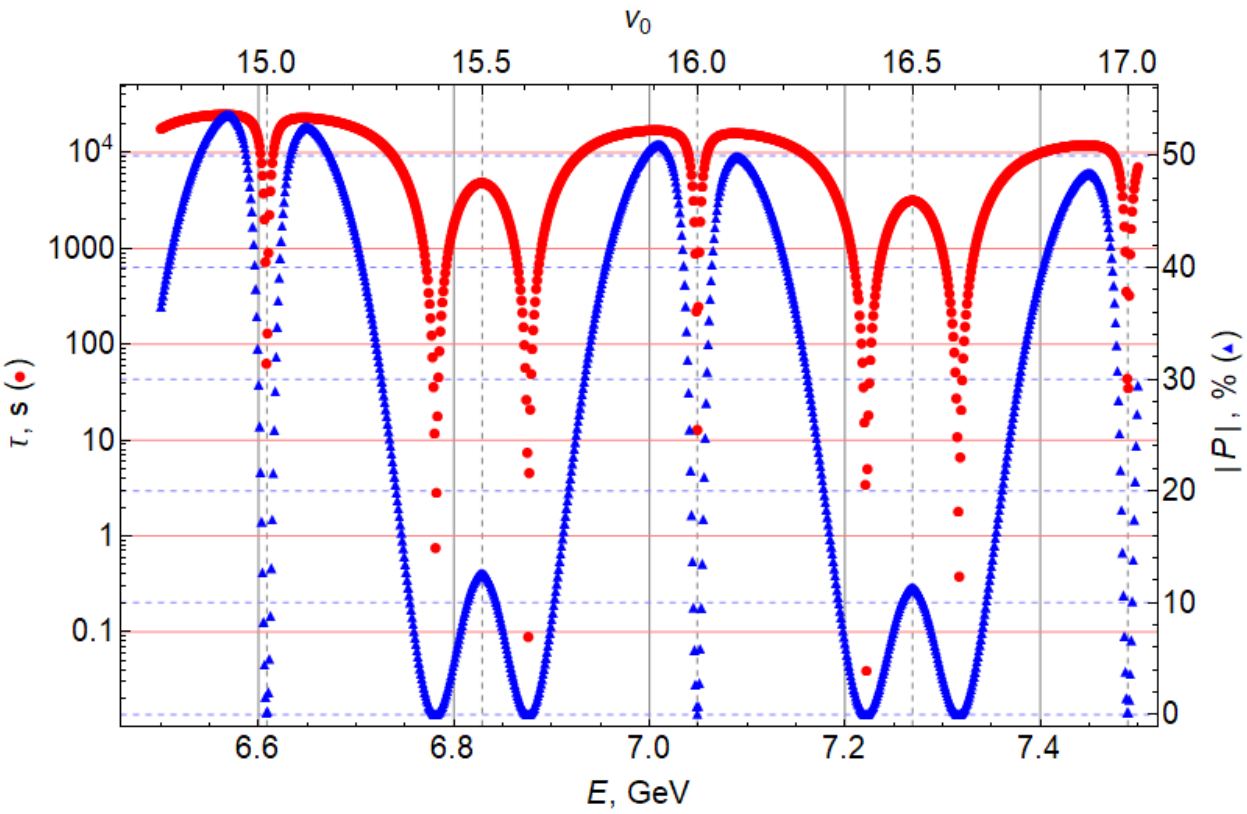

Fig.7 Dependence of the radiation spin relaxation time on energy with the rotator version from Table 3 with rotated extreme doublets of the lenses, see Fig. 5.

In principle, resonances with betatron frequencies can be made narrower. For this, it is necessary to fulfill the condition of the spin transparency of both: the rotator itself and the entire experimental straight section as a whole - from the rotator to the rotator [11]. But, as our study has shown, the fulfillment of the conditions for spin transparency requires several times stronger lenses in comparison with the variants of rotator optics considered above. Therefore, we have come to a compromise variant of using relatively weak lenses providing, nevertheless, a sufficiently long spin relaxation time. Note that electrons with the opposite sign of polarization with respect to the equilibrium one dictated by the Sokolov-Ternov self-polarization mechanism will depolarize much faster, tending exponentially to their natural state with a positive degree of polarization shown by the blue curve in Fig. 7. Apparently, bunches of electrons with a negative sign of polarization need to be updated more often so that their degree of polarization averaged over time is as high as for its positive sign.

Unfortunately, all programs of accelerator optics calculations available to us, such as MADx or RING, as well as the program for calculating the spin response functions ASPIRRIN, do not support the calculation of matrices of optical elements with combined longitudinal and quadrupole fields. Therefore, to calculate the time and degree of self-polarization in the variant of optics with combined longitudinal and quadrupole fields, we replaced the structure of rotators with a continuous longitudinal field (Table 4) with a structure similar to it presented in Table 5. In this structure, longitudinal field discontinuities are made, in which somewhat shortened lenses are located at the same distances from each other between their centers, as in the variant of Table 4, see Fig. 8. The presence of four families of quadrupole lenses and complete freedom in choosing the angles of their rotation around the axis make it possible to obtain any betatron phase advances and periodic beta functions of the rotator, both with the

longitudinal field turned on and off. We reproduced the X-box matrix the same as the rotator shown in Fig. 5.

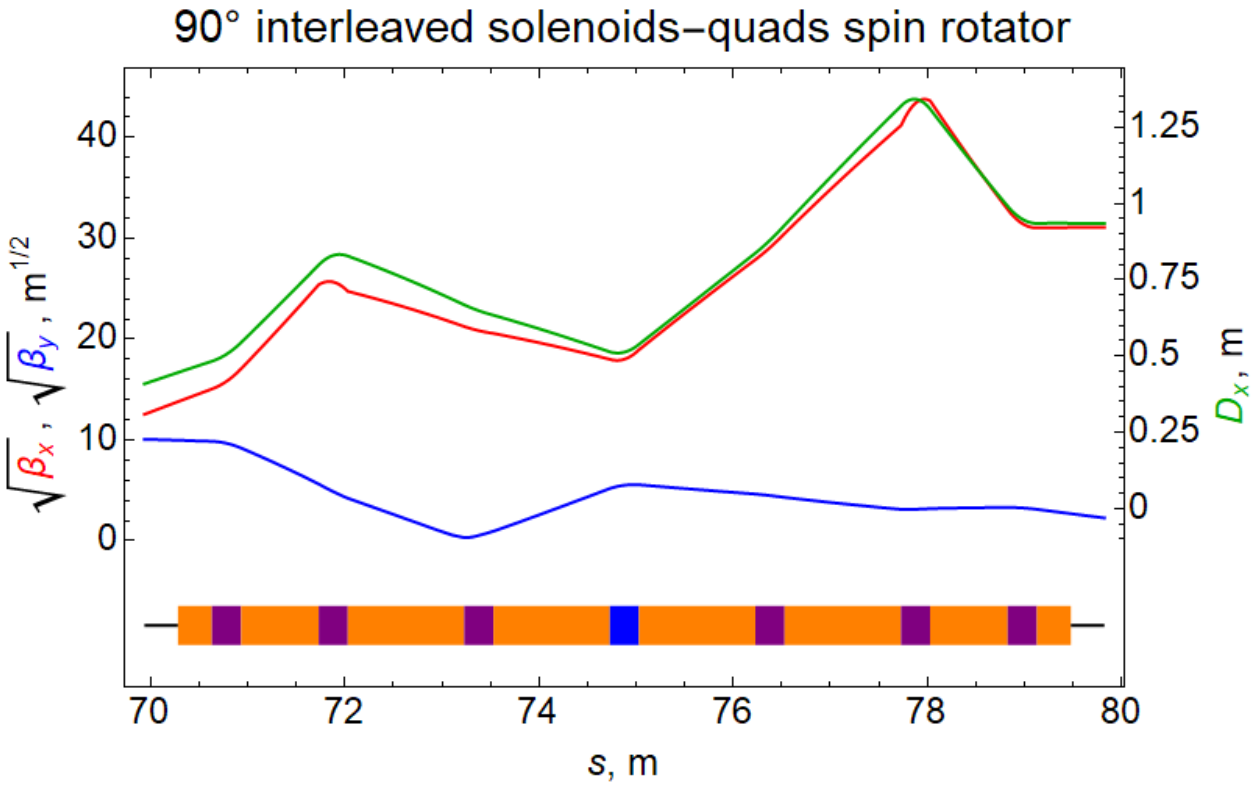

Fig.8 Amplitude functions in a rotator with alternating sections of solenoids and quadrupole lenses rotated around the axis.

Table 5. Parameters of lenses and solenoids of a spin rotator with alternating solenoidal and quadrupole fields for BR = 23.3495 T·m (E = 7.15 GeV).

Element and its sequence number	Length, m	Field or Gradient: T, T/m
Drift #1, #17	0.34556	$B_s = G = 0$
Solenoid #2, #16	0.35	$B_s = 5.15983$
Quadrupole: #3, #15	0.3	-41.5055 $(\varphi 3 = -\varphi 15 = -20.25818^0)$
Solenoid #4, #14	0.8	$B_s = 5.15983$
Quadrupole : #5, #13	0.3	45.5005 $(\varphi 5 = -\varphi 13 = -15.19364^0)$
Solenoid #6, #12	1.2	$B_s = 5.15983$
Quadrupole : #7, #11	0.3	-7.56501 $(\varphi 7 = -\varphi 11 = -7.59682^0)$
Solenoid #8, 10	1.2	$B_s = 5.15983$
Quadrupole : #9	0.3	-53.2734 $(\varphi 9 = 0)$

The magnitude of the modulus of the spin-orbit coupling vector calculated by the ASPIRRIN program is shown in Fig. 9. Its average value in the main part of the ring is less than one and it can be seen that this version of the rotator optics is the best of all those presented earlier. This was reflected in a significant increase in the spin relaxation time: $\tau_{rad} = 18800$ s versus 10000 s for the rotator version from Table 3. Both these tau-values are given for beam energy E = 7.15 GeV. The degree of equilibrium polarization also increased from P = 40% to P = 60%. The graphs of the dependence of the relaxation time and the equilibrium degree of polarization on energy

are shown in Fig. 10. We believe that the above estimates of radiative self-polarization refer not only to the version from Table 5, but also to the version of the parameters taken from Table 4 with a continuous longitudinal field.

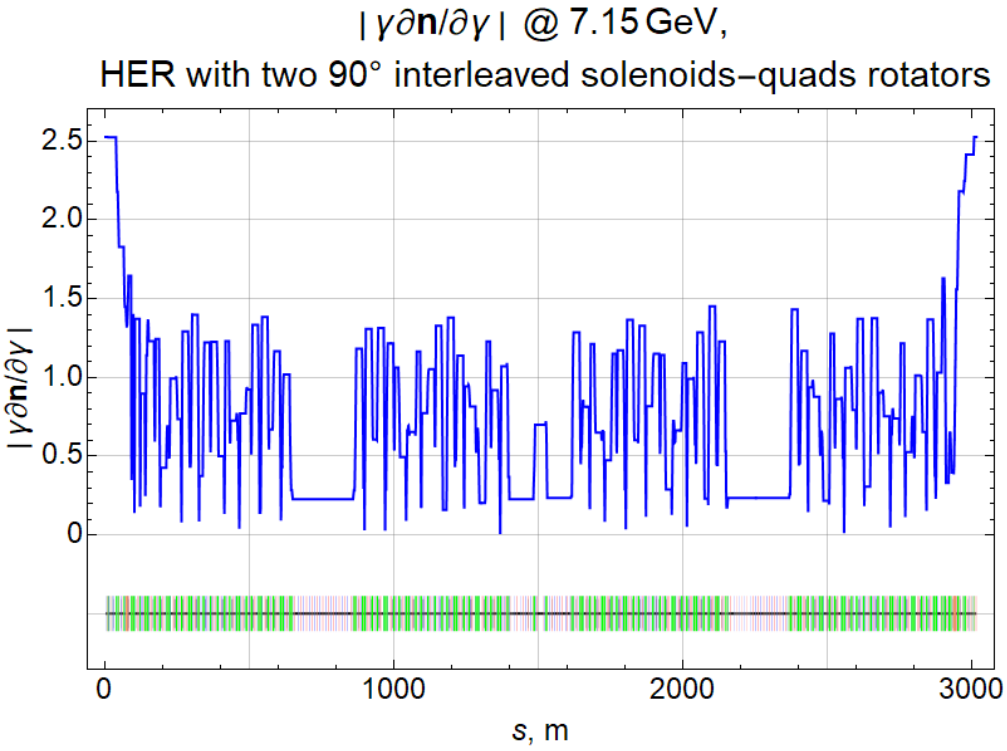

Fig.9 Modulus of the spin-orbit coupling vector in the HER ring with the rotator parameters from Table 5.

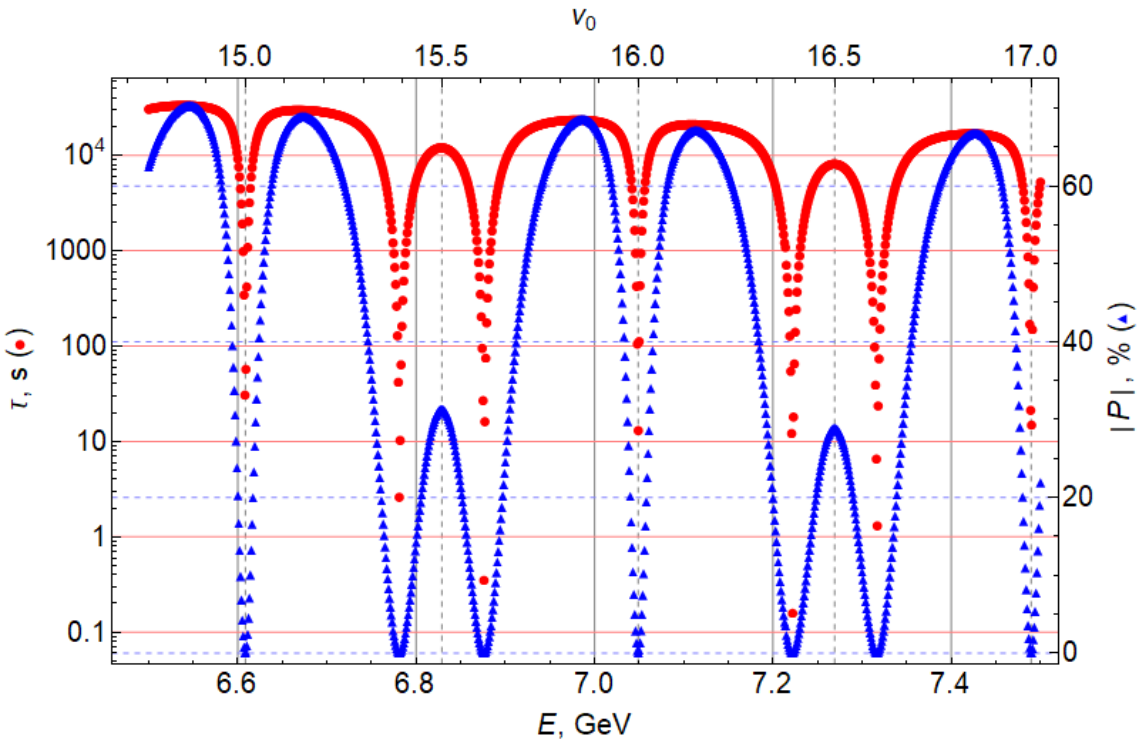

Fig 10. Radiation spin relaxation time and equilibrium degree of polarization versus energy for the rotator optics option from Table 5.

Finally, Figures 11-12 show the optical functions of the left and right halves of the long experimental straight section. They show spin rotators with an optical structure from Table 3. Outside the rotators, the beta functions and the dispersion function are the same for all the versions considered above, since the transport matrices of all these versions are made the same.

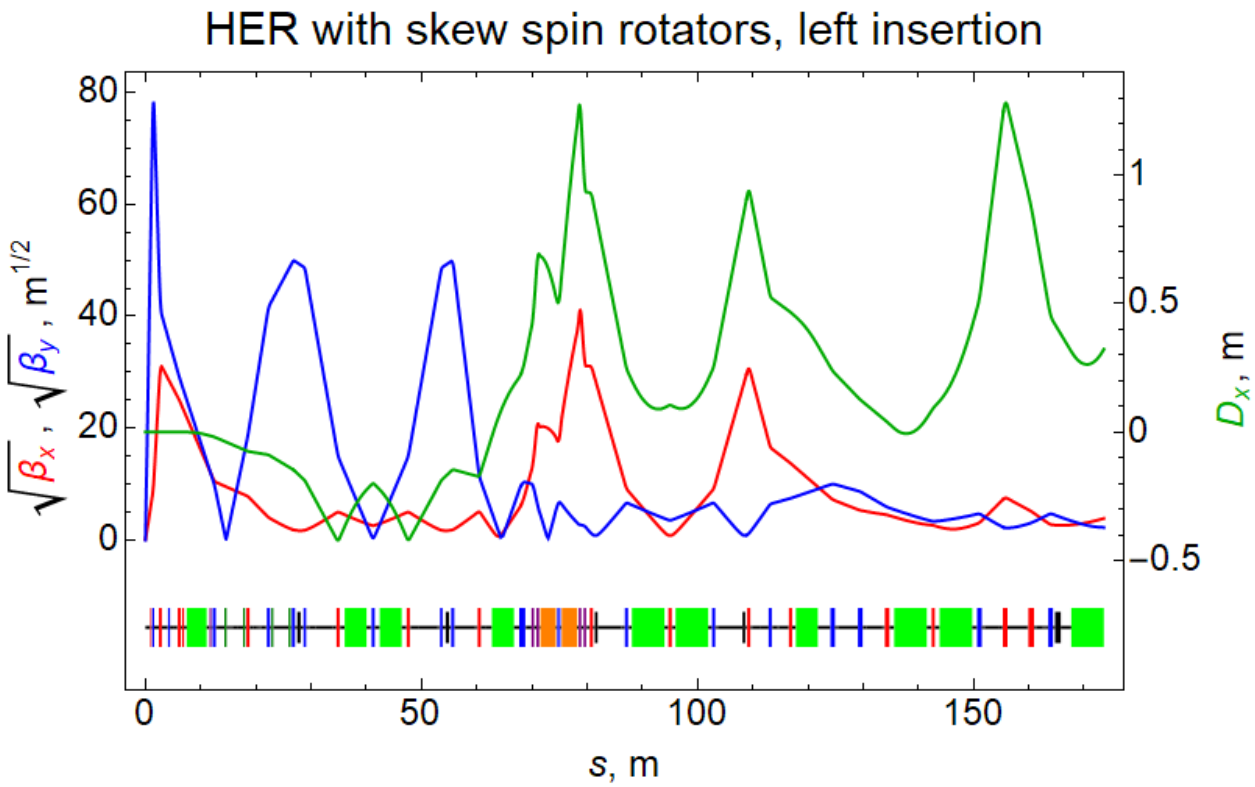

Fig. 11 Optical functions of the left half of the long experimental section.

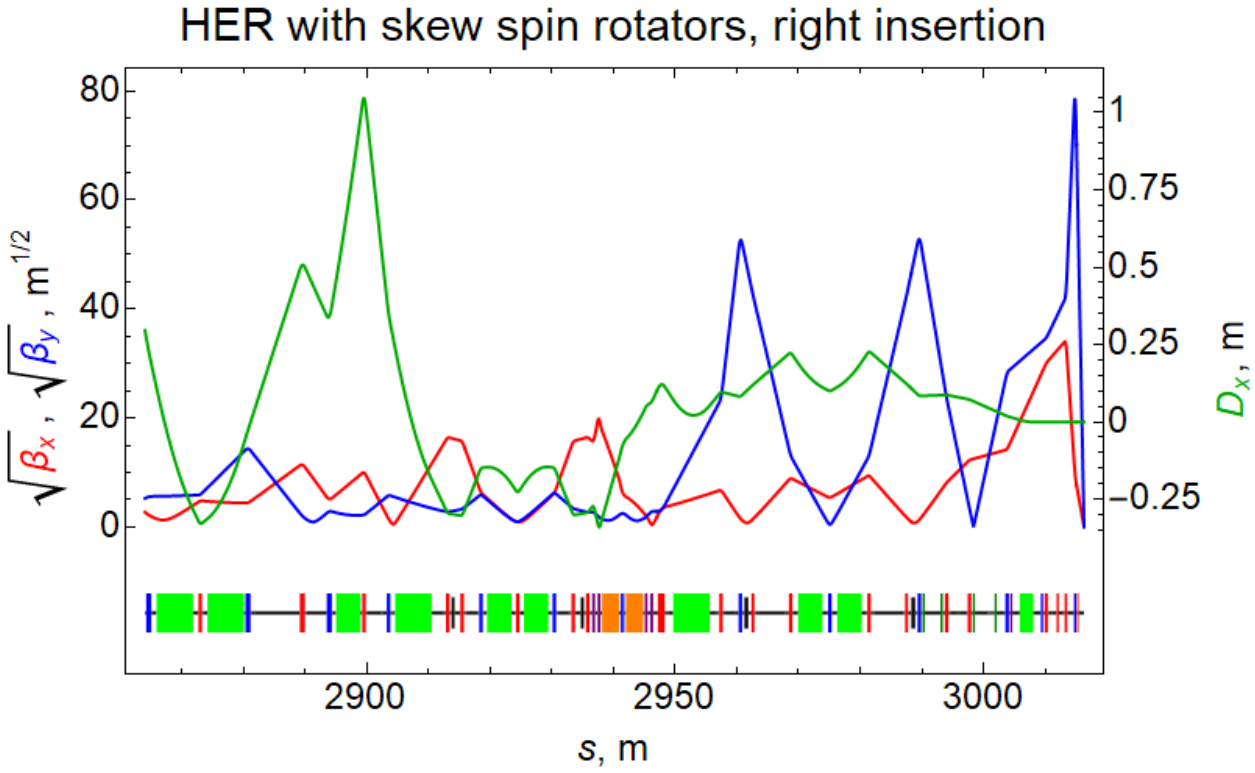

Fig. 12 Optical functions of the right half of the long experimental section.

Conclusion.

We found, in our opinion, an acceptable variant of converting the geometry of electron beam bends in the experimental section of the HER storage ring, which provides drift gaps with a length of about 10 meters for installing spin rotators in them. Two rotators serve to rotate electron spins by 90^0 from vertical to horizontal and then, after passing the crossing point, back to vertical.

Various lattice options for spin rotators are considered. In the variant with separate longitudinal and quadrupole transverse fields, the optimal transport matrix of the rotator was found, which made it possible to minimize the disturbances in the optics of the storage ring by the changes introduced. The disadvantage of this option is the relatively large value of the longitudinal magnetic field: over 6.54 T. This disadvantage is eliminated in the variant with the superposition of the rotated quadrupole fields on the continuous longitudinal field of the solenoid, which now occupies the entire length of the gap allocated for the rotator. The value of the longitudinal field in this variant dropped to 4.067 T.

Calculations of the relaxation time of polarization from the initial + 90% or -90% to its equilibrium value near + 60% showed its sufficiently large value, about 19000 sec, which will make it possible to have a very high level of average polarization during the lifetime of the beam with continuous feeding with new polarized electrons from injector.

The urgent task at the next stage is to check the boundaries of the dynamic aperture by tracking the particles in order to get an answer to the question of whether it has worsened in comparison with the initial version of the ring optics.

References.

[1] M. Roney, “Polarized Electron Beams in a SuperKEKB Upgrade”, e- Polarization Session

B2GM 34, KEK, 23 August 2019.

[2] Y. Ohnishi, H. Koiso, A. Morita, H. Sugimoto, and K. Oide, “LATTICE DESIGN OF LOW EMITTANCE AND LOW BETA FUNCTION AT COLLISION POINT FOR SuperKEKB”, Proceedings of IPAC2011, San Sebastián, Spain THPZ007.

[3] Y. Onishi on behalf of the SuperKEKB accelerator group, “Start of SuperKEKB”, 38th International Conference on High Energy Physics 3-10 August 2016 Chicago, USA. Published in PoS ICHEP2016 (2016) 006, pp.8.

[4] I. Koop, A. Otboev and Yu. Shatunov, “Issues and Challenges for Longitudinal Polarization in SuperKEKB”, a talk given at BELLE-II Collaboration Meeting. February 2020, Tsukuba.

[5] U. Wienands, ANL-APS and N. Wang, U. of Illinois Urbana-Champaign (Lee Teng Student), “A Compact Spin Rotator”, 24-Jun-2020, Belle 2 GM.

[6] A.A. Zholents, V.N. Litvinenko, Preprint YAF 81-80 (1981), also in DESY-L-TRANS-289.

[7] G. Luijckx et al, “Polarized electrons in the AmPS storage ring”, Proc. of PAC1997, Vancouver, Canada, 1997, pp.1063-1065.

[8] V.I. Ptitsyn, PhD thesis, Novosibirsk, 1997, in Russian.

[9] V.I. Ptitsyn, Yu.M. Shatunov, S.R. Mane," Spin response formalism in circular accelerators", Nuclear Instruments and Methods in Physics Research A 608 (2009) 225–233.

[10] Ya.S.Derbenev, A.M.Kondratenko, "Polarization kinematics of particles in storage rings", Sov.Phys.JETP 37:968-973, 1973, Zh.Eksp.Teor.Fiz.64:1918-1929, 1973.

[11] I. A. Koop, A. V. Otboyev, P. Yu. Shatunov, and Yu. M. Shatunov, "Spin transparent Siberian Snake and Spin Rotator with solenoids", SPIN-2006, Kyoto, AIP Conference Proceedings 915, 948 (2007).